Salt-mediated inactivation of influenza A virus in 1-µl droplets exhibits exponential dependence on NaCl molality

Aline Schaub[1], Beiping Luo[2], Shannon C. David[1], Irina Glas[3], Liviana K. Klein[2], Laura Costa[1,4], Céline Terrettaz[1,4], Nir Bluvshtein[2], Ghislain Motos[4], Kalliopi Violaki[4], Marie Pohl[3], Walter Hugentobler[4], Athanasios Nenes[4,5], Silke Stertz[3], Ulrich K. Krieger[2], Thomas Peter[2], Tamar Kohn[1]*

[1]Environmental Chemistry Laboratory, School of Architecture, Civil & Environmental Engineering, École Polytechnique Fédérale de Lausanne, Lausanne, Switzerland

[2]Institute for Atmospheric and Climate Science, ETH Zurich, Zurich, Switzerland

[3]Institute of Medical Virology, University of Zurich, Zurich, Switzerland

[4]Laboratory of Atmospheric Processes and their Impacts, School of Architecture, Civil & Environmental Engineering, École Polytechnique Fédérale de Lausanne, Lausanne, Switzerland

[5]Center for The Study of Air Quality and Climate Change, Institute of Chemical Engineering Sciences, Foundation for Research and Technology Hellas, Patras, Greece

*Correspondence: tamar.kohn@epfl.ch

Abstract

Influenza A virus (IAV) spreads through airborne particles ranging from sub-micrometer to millimeter-sized droplets. The stability of airborne IAV remains difficult to estimate and depends, among others, on the respiratory matrix composition and the size-dependent drying kinetics. Here, we combine experiments on deposited millimeter-sized saline droplets with a biophysical aerosol model to quantify the effect of NaCl on IAV stability, in the presence and absence of sucrose as organic co-solute. We demonstrate that IAV inactivation in dilute saline droplets after exposure to air at various relative humidities is driven by the increasing NaCl molality during water evaporation, rather than by efflorescence, i.e. the precipitation of salt crystals. For pure aqueous NaCl droplets, we find the inactivation rate constant to depend exponentially on NaCl molality, which enables us to simulate inactivation under both efflorescing and deliquescing conditions. We provide evidence for virion integrity loss as the primary inactivation mechanism. Addition of sucrose attenuates IAV inactivation, which we attribute to two mechanisms: first, sucrose decreases the NaCl molality during the drying phase, and second, at equal NaCl molality, sucrose shields IAV from the inactivating effects of NaCl. These experiments help advance our understanding of IAV stability in expiratory particles and the associated transmission risks.

Keywords: Influenza A virus – Expiratory droplet – Salinity – Virus inactivation – airborne transmission

Introduction

Respiratory viruses such as influenza A virus (IAV) can be transmitted by expiratory aerosol particles and droplets emitted by an infected individual.[1–5] Small particles (up to tens of µm) can stay airborne for minutes hours[6] and travel dozens of meters before encountering a new host,[7] while larger droplets (> 100 µm) can travel only a short distance (1-2 m) and settle within seconds.[7] For both aerosol particles and droplets, IAV can only be transmitted if the viruses remain infectious outside the host. Understanding the environmental parameters that modulate IAV infectivity in expiratory particles and droplets is therefore crucial to tackle seasonal flu epidemics as well as worldwide pandemics.

When particles and droplets are exhaled from the respiratory tract, they leave an environment with a relative humidity (RH) close to 100% and body temperature and enter a cooler, dryer environment. In typical indoor environments in temperate climates, RH can be as low as 30% during winter, whereas it is around 50% in summer.[8] The RH,[9–19] the temperature,[20–22] and the initial size and composition of the expiratory particle[23–25] dictate the droplet drying rate and hence the concentration of solutes in the droplets. If the RH is below the efflorescence relative humidity (ERH) of the salts, the salts will effloresce. Moreover, gas exchange with the environment takes place,[25] and liquid-liquid phase separation may occur.[26] These processes modulate the salinity as well as the pH within the particle. We previously found that the pH in small aerosol particles rapidly decreases to around 4 as a result of gas exchange with the surrounding air.[27] This low pH was suggested to be a primary driver of IAV inactivation in aerosol particles in indoor environments.[27,28] In contrast, larger droplets (> 100 µm) undergo a much slower acidification (on the scale of hours), suggesting that IAV inactivation observed in droplets is driven by another factor.

Previous studies have suggested an important contribution of salt to virus inactivation in deposited droplets. Specifically, the stability of IAV,[29] bacteriophage MS2,[19] and SARS-CoV-2[20] was found to be low at intermediate RH (50-65%), just above ERH of NaCl (41-51%),[30] where the salinity in the droplets is expected to be maximal. In search for a mechanistic explanation for this observation, Lin and Marr[19] suggested that the cumulative dose (NaCl concentration multiplied by exposure time) of NaCl over a 1-h drying period is the main determinant of virus inactivation in droplets and aerosol particles for bacteriophages MS2 and Φ6. Similarly, Niazi et al.[31,32] showed that rapid evaporation and hence rapid efflorescence stabilizes IAV and human rhinovirus-16 in airborne aerosol particles, suggesting that increased stability is due to a shorter exposure to high salinity. An important role of evaporation dynamics on IAV inactivation in droplets was also proposed by French et al.,[23] who observed faster inactivation during the initial evaporation step, while the particle is still liquid, and a slower decay after efflorescence. Likewise, a near-instantaneous 50% loss in SARS-CoV-2 infectivity was observed to be associated with efflorescence, followed by a slower inactivation rate.[33,34] Besides salt efflorescence, IAV stability is also dependent on the presence of organic co-solutes in the matrix, which are typically reported to exert protective effects,[29,35] though the underlying mechanisms are not

understood. Nevertheless, some organic compounds, such as the saliva constituents lysozyme and lactoferrin, are viricidal and can enhance viral inactivation.[36,37] Finally, Rockey et al.[38] observed a lower IAV stability in saliva droplets than in respiratory mucus droplets, whereby the difference could not be explained by the salt content nor the drying kinetics, but was instead attributed to the morphology of the dried droplets. Overall, the role of salinity, efflorescence and organic co-solutes in IAV inactivation is thus not fully understood, and it remains difficult to predict inactivation in saline droplets, in particular in the presence of organics.

The goal of this study was to enable the estimation of IAV infectivity in drying saline droplets and to unravel the role of organics in modulating salt-mediated inactivation. While working with real respiratory matrices is the gold standard, we here aimed to ensure tight control on salinity and organic content in our experiments. We therefore chose to work with a model matrix consisting of NaCl at physiological concentration, and sucrose as an organic substance that can modulate the occurrence of efflorescence. We monitored the inactivation of influenza virus strain A/WSN/33 in 1- and 2-µl drying droplets containing NaCl and sucrose at different ratios. This droplet size was chosen to represent the size of the large particles emitted while speaking and coughing.[39] Inactivation and droplet drying kinetics were monitored over time and subsequently modeled as a function of NaCl molality using ResAM, a biophysical aerosol model. We demonstrate that IAV inactivation is a function of NaCl molality, and that sucrose exerts a dual protective effect by maintaining lower salinity during the initial drying phase, and by protecting the virions against the detrimental effects of salt.

Materials and methods

Virus propagation, purification and enumeration

Influenza A virus (IAV) strain A/WSN/33 (H1N1 subtype) was propagated and purified as previously described.[27] Details are provided in the Supporting Information (SI). Virus infectivity was quantified as plaque forming units (PFU)/ml and total virus concentration was quantified as genome copies (GC)/ml by RT-qPCR as detailed in the SI. All RT-qPCR procedures followed MIQE guidelines[40] (see **Table S1**).

Virus inactivation experiments in droplets

Experiments were conducted in solution with an initial composition of either 8 g/l (0.14 molal (*m*)) NaCl solution (ThermoFisher Scientific, 207790010), 5.8 g/l (0.14 *m*) LiCl solution (Acros Organics, 193370010), or 8 g/l NaCl solution supplemented with either 8 (0.023 *m*) or 64 g/l (0.187 *m*) of sucrose (Fisher BioReagents, BP220-1). The solutions were all prepared using milli-Q water. Purified virus stock in PBS was spiked in 100 µl of the matrix in a 1.5-ml plastic tube (Sarstedt, 3080521), to achieve a starting concentration in the experimental solution of either 10^7 PFU/ml ("normal titer) or 10^9 PFU/ml ("high titer"). The tube was vortexed and kept in a cold tube rack until use.

Experiments were conducted in NaCl and sucrose matrices. All information concerning matrix preparation are available in the SI. Inactivation experiments were performed in an environmental chamber (Electro-Tech Systems, 5532) with controlled relative humidity and temperature. Prior to the experiment, the chamber was set at the targeted RH and room temperature (25°C ± 2) and left to equilibrate. Once equilibrated, 1- or 2-µl droplets were deposited in the wells of a 96-well plate with a non-binding surface (Greiner Bio-One, 655901), one droplet per well. Droplets were then left to dry at 30% or 65% RH (unless mentioned otherwise), and were periodically collected (see below) over the course of up to 180 min. For each time point in an experiment, three droplets were collected. The three droplets that were deposited last were sampled immediately to act as the time = 0 (t0) sample. The deposition time (~10 s per droplet) was recorded and accounted for when sampling the time points. In each experiment, a control was performed in bulk.

To sample the droplet, 300 µl of PBSi were added to the well. The droplet was then resuspended by scratching the bottom of the well with a 200-µl pipette for 5 s, followed by up and down pipetting for 5 times, and a second scratching + mixing cycle was done. The scratching was added to the procedure to ensure the detachment of the virus from the surface, and the mixing was used to ensure a homogeneous solution. Then, each sample was aliquoted in 2x 150 µl and frozen at -20°C until further quantification by culturing and RT-qPCR. In each experiment, a control was included by sampling 1 µl of the experimental solution directly from the plastic tube at the beginning and at the end of the experiment. The sample was immediately diluted in 300 µl of PBSi. The tube was kept in the environmental chamber during the whole experiment to ensure similar conditions as for the droplets.

To account for physical loss of the virus due to attachment to the wells, recovery of the total (infectious plus inactivated) virus from the plate was measured by RT-qPCR. The measured inactivation was then corrected for virus recovery to determine the actual inactivation.

Virus inactivation experiments in bulk

Inactivation in NaCl bulk solutions were performed in triplicate at room temperature, at three different NaCl concentrations (0.14 *m*, 2.8 *m* and 6.1 *m* – saturated). A purified virus stock in PBS was spiked in 1 ml of each matrix in a 1.5-ml plastic tube to achieve a starting concentration in the experimental solution of 10^7 PFU/ml. The tubes were vortexed and a 5-µl sample was taken immediately, and diluted in 495 µl of PBSi. Samples were taken every 2 h for 10 h, and a final time point was taken after 24 h. All the samples were frozen at -20°C immediately after sampling until quantification.

Determination of inactivation rate constant

Inactivation rate constants of each experimental condition were determined from least square fits to the log-linear portion of the inactivation curve (that is, for droplets, the inactivation occurring in equilibrated droplets, i.e. ≥ 40 min after deposition), assuming first order kinetics,

$$\ln\frac{C}{C_0} = -k \cdot t$$

Equation 1

Here, C is the virus titer at time t, C_0 is initial virus titer and k is the inactivation rate constant. All replicate experiments of a given experimental condition were pooled. 99%-inactivation times (t_{99}) were determined based on k:

$$t_{99} = -\frac{\ln(0.01)}{k}$$

Equation 2

Rate constants and associated 95% confidence intervals were determined using GraphPad Prism v.10.0.2.

Determination of evaporating droplet radius

The evaporation of the droplets was filmed by a Raspberry Pi 4 computer (Model B Rev. 1.4) and a camera (Sony IMX477R) connected to a power bank (Varta). The camera was positioned 15 cm above the well plate and took a picture every 16 s. The size of each droplet was calculated from the pictures using the software ImageJ (version 1.53t).

Biophysical modeling

We used the Respiratory Aerosol Model ResAM, to predict NaCl and sucrose concentrations within the evaporating droplets and to simulate the inactivation kinetics of IAV. ResAM is a spherical shell diffusion model used to determine viral inactivation in droplets, considering their initial composition and size, as well as the relative humidity, temperature and ventilation in the experimental chamber. ResAM is fully described by Luo et al.[27] and the adaptation to droplet modeling is described in detail in the SI.

Results

IAV inactivation kinetics in efflorescing NaCl droplets

Inactivation kinetics of IAV in 1- and 2-µl aqueous NaCl droplets exposed to an RH of 30% were measured over the course of 60 min, to compare the kinetics in two different droplet sizes. Simultaneously, the droplet size was monitored as a function of time by videography (**Figure 1**). Initially, the droplets were composed of 8 g/l of NaCl, and 1% (v/v) of infectious virus in phosphate buffer saline (PBS), reaching a virus titer of 10^7 PFU/ml. Following deposition, the droplets shrank slowly until salts visibly effloresced after approximately 20 min (1-µl droplets) and 36 min (2-µl droplets), respectively (**Figure 1A-B**). After efflorescence, the appearance of the droplets , as seen by eye and videography, did not change until the end of the experiment.

The inactivation curve of IAV in both droplet sizes initially followed the evaporation kinetics of the droplets and exhibited an inverted sigmoidal shape (**Figure 1C-D**): during the initial phase of exposure to the controlled RH in the gas phase, the volume loss of the droplets was largest because of the sizable humidity gradient between the air directly above the liquid surfaces and the prescribed RH in the environmental chamber. However, during the initial 5-15 min, the camera barely detected any change in droplet size (**Figure 1A-B**). This is probably because the droplets flattened out, while the covered surface remained constant, which cannot be seen from the elevated angle of the camera.

Despite the continuous decrease in volume and the increasing salt concentration, IAV remained infectious during the first 15-25 min. This was followed by a short phase of about 5 min during which IAV infectivity plummeted by more than 2-$\log_{10}$. After efflorescence, the inactivation kinetics slowed significantly and showed a constant inactivation rate for the remainder of the experiment, resulting in less than 2-$\log_{10}$ inactivation in the 40 min after efflorescence. In 2-µl droplets, inactivation kinetics were similar to 1-µl, although the initial slow inactivation phase was prolonged to approximately 30 min, due to the smaller relative volume change rate and hence the later efflorescence of the larger droplets. Control experiments conducted in bulk solutions (see Supporting Methods) showed only minor inactivation during the course of the experiment, suggesting that the observed inactivation can be attributed to the droplet environment.

Two mechanisms may explain the inverted sigmoidal inactivation kinetics: first, the rapid drop off in virus titer may be caused by the formation of salt crystals during efflorescence, as suggested in the context of influenza vaccine microneedles[41] and salt-coated filters on surgical masks.[42] Alternatively, inactivation may be driven by IAV exposure to high salinity, which mirrors virus inactivation in the droplets. Specifically, NaCl molality increases as the droplet evaporates and supersaturation is reached prior to efflorescence, exposing the virus to high salinity, before the salinity decreases to saturation level due to efflorescence. The latter mechanism is supported by our finding that substantial inactivation occurs before efflorescence becomes visible by eye, suggesting that high salinity drives inactivation.

Furthermore, **Figure 1C-D** suggests that the data scatter is small before efflorescence, but large afterwards. This observation is also consistent with salinity being the main driver of inactivation: the fastest inactivation occurs under the most saline conditions just before efflorescence, and because efflorescence is a stochastic nucleation process, different droplets effloresce at slightly different times. As a consequence, the viruses in these different droplets are exposed to differently high salt concentrations, resulting in different titers in the moment of efflorescence and beyond.

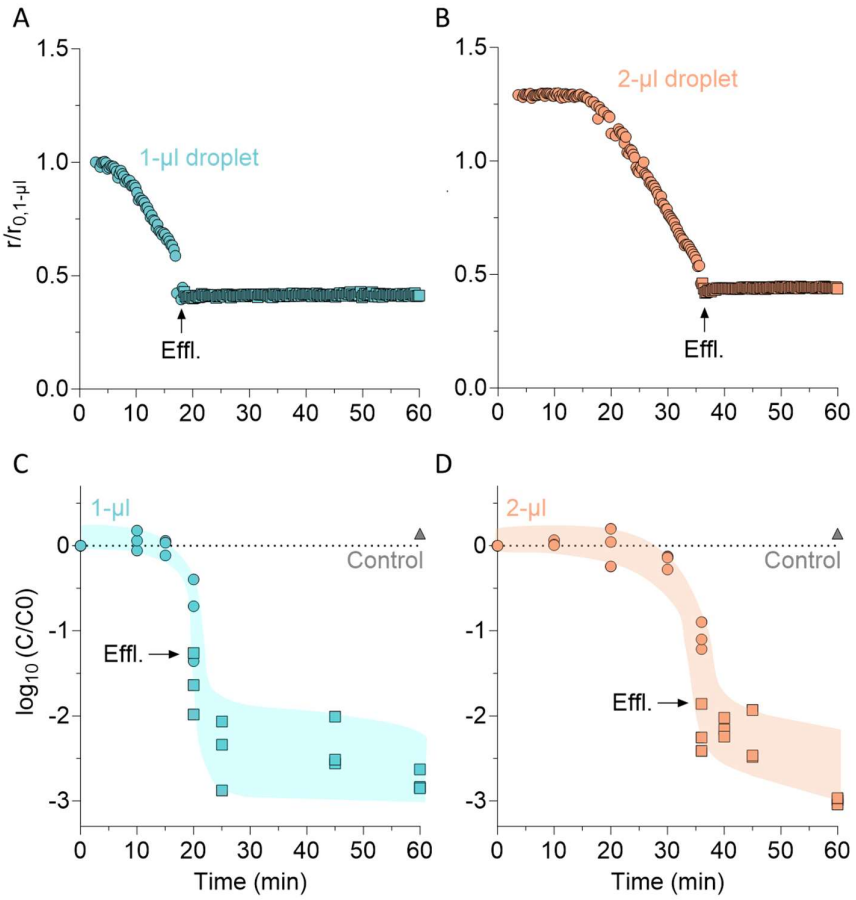

Figure 1: Water loss of highly diluted 1-µl and 2-µl aqueous NaCl droplets exposed to 30% RH and concomitant inactivation of IAV in these droplets. (A,B) Relative droplet radius versus time for one individual droplet, first decreasing due to evaporation, then constant after efflorescence occurred (marked by upward arrows). The droplet radius (r) was determined by video recording paired with ImageJ analysis and normalized by the initial radius of the 1-µl droplet ($r_{0,1\text{-µl}}$). The measurements are representative of triplicate droplets. (C,D) Inactivation of IAV in drying droplets. Each data point represents one individual droplet, with circles for liquid droplets and squares for effloresced droplets. Shadings are meant to guide the eye, showing small data scatter before and large data scatter after efflorescence. Gray triangles represent control experiments conducted in bulk solution.

IAV inactivation kinetics in non-efflorescing NaCl droplets

To confirm that the main driver of inactivation is high salinity, we tested IAV inactivation under experimental conditions of increasing salt molality but in the absence of efflorescence (**Figure 2A**). First, experiments were conducted in the same NaCl matrix as in **Figure 1**, but at RH = 65% ≫ ERH. Second, inactivation was measured at RH = 30% (same as in **Figure 1**), but in a matrix containing LiCl instead of NaCl. LiCl has an ERH of 1-4%,[30] and therefore remains deliquesced at 30% RH. As a reference, experiments in NaCl droplets at 30% RH were included. In this set of experiments, the initial virus titer was increased by 2-$\log_{10}$ compared to the experiments shown in **Figure 1**, in order to increase the detection range. The initial LiCl molal concentration (0.14 m) was identical to the NaCl molal concentration.

The inactivation in NaCl droplets at 30% RH followed kinetics comparable to those shown in **Figure 1**, though efflorescence occurred approximately 5 min earlier than in experiments with a lower titer (15 min after deposition instead of 20 min, respectively). This suggests that the presence of concentrated virus can trigger efflorescence (**Figure S1Erreur ! Source du renvoi introuvable.**). The first-order inactivation rate constant (k) after efflorescence (time after deposition ≥ 40 min) was 1.8 (± 0.4)·10^{-2} min^{-1}, corresponding to a time to reach 99% inactivation (t_{99}) of 260 min (**Table S2**Erreur ! Source du renvoi introuvable.). As explained for **Figure 1C-D**, the large data scatter after efflorescence is to be expected owing to the stochastic nature of the heterogeneous nucleation process.

The viral infectivity in NaCl droplets at 65% remained stable during 20 min after deposition, consistent with initial conditions of high dilution. Subsequently, it exhibited a first-order inactivation with a rate constant k = 6.5 (± 0.4)·10^{-2} min^{-1}, corresponding to $t_{99} \approx 71$ min (**Table S2**Erreur ! Source du renvoi introuvable.). After 120 min, IAV inactivation in droplets dried at 30% and 65% RH reached a similar level. In contrast, LiCl droplets at 30% RH exhibited a rapid drop in IAV titer between 10 and 20 min, similar to the time scale in NaCl droplets at the same RH. However, the titer dropped more extensively, and inactivation reached > 5-$\log_{10}$ after 30 min. Thereafter, a reduction in the inactivation rate was observed until 60 min, after which the viral titer was no longer quantifiable. Note that decelerating inactivation curves are often observed in experiments leading to a high titer reduction, and may be explained by the presence of viral aggregates.[43,44] As expected, no efflorescence occurred in the LiCl droplets. Combined, these experiments suggest that high salt molality rather than the formation of salt crystals drives inactivation.

IAV inactivation kinetics in NaCl/sucrose droplets

To assess the inactivation of IAV in the presence of organics, sucrose was added to the NaCl solution. Organics have previously been observed to be protective for IAV in bulk solutions,[27] deposited droplets,[29] or airborne aerosol particles.[35] In these studies, however, the protective matrix was a complex mixture of organics. Here, we chose to use a simple NaCl/sucrose/water system, to be able to determine the concentration of the solutes along the experiment using a biophysical aerosol model (see below). Based on droplet efflorescence

analysis (**Figure S2**), NaCl:sucrose mass ratios of 1:1 and 1:8 were selected (corresponding to 8 and 64 g/l of sucrose, respectively), providing conditions where crystallization was permitted (1:1) and prevented (1:8), as determined by eye and videography. The inactivation kinetics of IAV in these two NaCl/sucrose matrices were compared with the inactivation in pure NaCl droplets at 30% RH, here denoted NaCl:sucrose 1:0.

After deposition, the 1:1 NaCl:sucrose droplets started shrinking until efflorescence, after 18 min (**Figure 2B**). The inactivation kinetics exhibited an inverted sigmoidal shape, with a fast decay around efflorescence followed by a tail (**Figure 2C**), where slow first-order inactivation continued until conclusion of the experiment. The inactivation kinetics were similar to those observed in 1:0 droplets, though efflorescence in the 1:1 droplets occurred 3 min later and was associated with a larger droplet radius, a smaller drop in titer and a slower first-order inactivation rate constant in the tail ($1.8 (\pm 0.4)\cdot10^{-2}$ min^{-1} vs. $7.6 (\pm 3.3)\cdot10^{-3}$ min^{-1} for 1:0 and 1:1 ratios, respectively (**Table S2**Erreur ! Source du renvoi introuvable.)). The 1:8 NaCl:sucrose droplets initially shrank at the same rate as the 1:1 droplets but then stabilized as liquid droplets with the largest relative radius (**Figure 2B**). The inactivation kinetics were slower than in the 1:0 and 1:1 droplets, reaching less than 1-log_{10} inactivation after 180 min, and an inactivation rate constant in the tail of $6.4 (\pm 1.7)\cdot10^{-3}$ min^{-1} (**Table S2**Erreur ! Source du renvoi introuvable.). In both sucrose-containing droplets, IAV was thus partially protected from NaCl-mediated inactivation, whereby the protection was greater at a higher sucrose content.

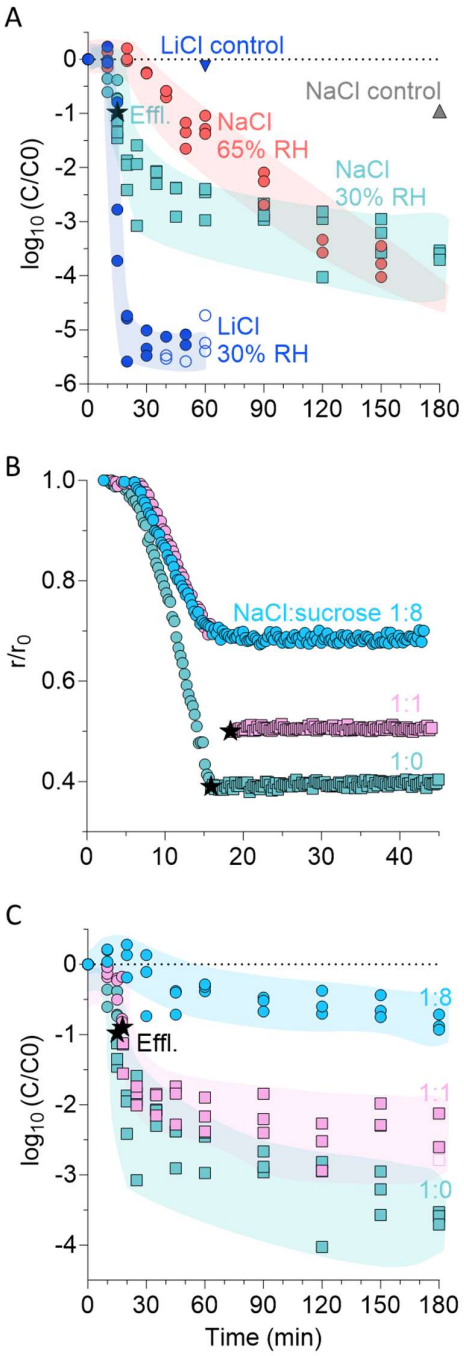

Figure 2: IAV inactivation in 1-µl NaCl, LiCl and NaCl:sucrose droplets. (A) Inactivation of IAV in 1-µl NaCl droplets at 30% RH and 65% RH for 180 min and in 1-µl LiCl droplets at 30% RH for 60 min. Efflorescence of NaCl droplets at 30% RH is represented by a black star (★).No efflorescence occurred in NaCl 65% RH and in LiCl 30% RH. (B-C) IAV inactivation in 1-µl droplets at 30% RH in various NaCl:sucrose mass ratios. (B) Droplet volume shrinkage due to water evaporation until efflorescence (★) or liquid-phase equilibrium with air. Radius (r) was determined by video recording paired with ImageJ analysis, and normalized by dividing by the initial radius of each droplet (r_0). (C) Inactivation of IAV in drying droplets versus time. Efflorescence occurred in NaCl:sucrose 1:0 and 1:1 and is represented by a black star (★). In NaCl:sucrose 1:8, efflorescence was not visible by eye nor videography. Data for NaCl 1:0 are the same in panels A and C. Each data point represents one individual droplet, with circles representing liquid droplets and squares representing effloresced droplets. Empty symbols indicate data below the limit of quantification. Triangles represent control in bulk. Shadings are meant to guide the eye.

Biophysical model of virus inactivation in drying NaCl/sucrose droplets

The biophysical model ResAM (Respiratory Aerosol Model) was used to simulate the water activity and composition within the droplet as a function of time. A full description of ResAM is available in Luo et al.,[27] and the modifications applied in this study are given in the Supporting Information. In brief, the model is based on a spherical shell diffusion system. However, the droplets in the present work are large (millimeter-sized) and not completely spherical, but to some degree spread out in the wells. Hence, consideration of their flattened shape is required. This is done by describing the flattened droplet with average thickness *h* as a hemispherical shell with equal thickness concentrically covering an inert core (see **Figure S3**). To inform the model, IAV inactivation was first parameterized in terms of the NaCl molality and sucrose content. Generally, while the conditions in the droplets change as a function of time, one cannot expect first order inactivation kinetics. Conversely, we assumed that droplets exhibiting first-order inactivation are in equilibrium with the surrounding air. This can occur, for instance, after efflorescence or when the viscosity of the droplets becomes high and the diffusivity within them is low, such that their salt molality no longer changes.

The dependence of inactivation on NaCl molality was determined based on data obtained in both droplet and bulk experiments. Specifically, the molality of any residual fluid in effloresced NaCl droplets following exposure to 30% RH corresponds to saturation molality, i.e. 6.1 mol NaCl / kg H_2O = 6.1 *m*,[45] whereas the molality in deliquesced droplets at 65% RH corresponds to a supersaturated state of ca. 8 *m*. In agreement with this molality difference, the IAV inactivation rate constant *k* in the residual fluid at 30% RH (after efflorescence) was lower than that measured at 65% (**Figure 2** and **Table S2**). To establish a relationship between NaCl molality and *k* over a wide molality range, we furthermore considered inactivation measured in bulk solutions of 0.14, 2.8 and 6.1 *m* NaCl (**Figure S4** and red dots in **Figure 3B**). Finally, the rate constant for saturated salt solutions (**Table S2**) was confirmed in a droplet experiment conducted in NaCl at 74% RH (**Figure S5**), where the NaCl molality in the equilibrated droplet corresponds to 6.1 *m*. Based on these data, the following relationship between NaCl molality and inactivation rate k (in s^{-1}) and corresponding e-folding time τ could be established (**Figure 3B**):

$$\frac{1}{\tau(m)} = k(m) = k_0 \cdot e^{m/m_0} ,$$

Equation 3

where m is the molality of NaCl (in mol/kg H_2O), m_0 is a fitting parameter corresponding to 2.095 mol/kg H_2O; and k_0 is the fitted inactivation rate constant in pure water, corresponding to $2.5 \cdot 10^{-5}$ s^{-1}.

For sucrose-containing droplets, a similar dependence of k on NaCl molality was assumed, though the absolute value of k at saturation molality was lower due to the protective effect of sucrose exerted in

equilibrated droplets (**Figure 2C**). To account for the effect of sucrose, the relationship shown in **Equation 3** was expanded as follows:

$$\frac{1}{\tau(m,x)} = k(m,x) = k_0\left\{1 + \left(e^{m/m_0} - 1\right) \cdot e^{-s_0\, x^{s_1}}\right\},$$

Equation 4

where x is the mole fraction of sucrose defined as $x = m_{\text{sucrose}}/(m + m_{\text{sucrose}})$, and s_0 = 1.8696 and s_1 = 0.19451 are constant coefficients. For $x = 0$, i.e. in the absence of sucrose, **Equation 4** reduces to **Equation 3**. The inactivation rate in pure water is k_0, while the impact of salt is given by the term $\left(e^{m/m_0} - 1\right)$ and protection effect by sucrose by the term $e^{-s_0\, x^{s_1}}$. The constant coefficients in **Equation 3** and **Equation 4**, k_0, m_0, s_0 and s_1, were determined by optimizing the output of ResAM to match the measured titers in the NaCl-sucrose solutions, see **Figure 3G-J**. This fitting procedure must also properly account for the diffusivities of H_2O molecules in these solutions (see **Figure 3A**). While appearing arbitrary at first glance, these constant coefficients are actually quite well constrained. Mapping the kink in the curves just before efflorescence (**Figure 3G-J**) is a challenge that effectively limits the fitting options (calculations not shown).

Next, ResAM was used to model the water activity and the NaCl molality in the different NaCl droplets. Hereby some assumptions were made: because the inactivation rate constant observed in the tail of the pure salt droplet at 30% RH corresponds to that of saturated NaCl solutions (as measured in bulk and in droplets at 74%; see **Figure 3A** and Supporting Information), we conclude that NaCl crystals grow around the virus, forming pockets that limit water evaporation and in which the aqueous salt is saturated. Furthermore, while the 1:8 NaCl:sucrose matrix does not show efflorescence visible by eye, the observed reduction in the inactivation rate after 45 min is indicative of efflorescence. We therefore assume that microscopic dendritic crystal growth occurred in this matrix. This assumption is needed to ensure that the model is consistent with the experimental data. Finally, the model assumes a homogeneous distribution of the virus in the droplet. This is in contrast with studies suggesting that the virus may preferentially localize on the border of the dried droplet when proteins are present in the matrix.[24,38] The exact location of IAV viruses in a drying NaCl/sucrose droplet remains to be assessed.

Under these assumptions, ResAM revealed the following: (i) at 65% RH, (**Figure 3C**) the NaCl molality increases up to 8 *m*, until equilibrium with air. No efflorescence occurs at this RH, such that the droplet remains supersaturated in NaCl; (ii) at 30% RH (**Figure 3D**), NaCl molality first increases due to water evaporation, and reaches supersaturation (up to 20 *m* at the particle surface) before the salt effloresces. After efflorescence, the concentration drops down to saturation molality (i.e., 6.1 *m*); and (iii) in sucrose-containing droplets at 30% RH, the NaCl molality prior to efflorescence is dependent on the sucrose content; the more sucrose, the lower NaCl molality (**Figure 3D-F**). After efflorescence, the remaining aqueous NaCl

molality corresponds to saturation, i.e. 6.1 *m*, in all matrices. The water activities within the drying droplets are shown in **Figure S6.** The diffusion coefficient of water in the different NaCl:sucrose matrices are shown in **Figure 3A**.

Finally, by combining the simulated NaCl molality and the molality- and sucrose-dependent inactivation rate constant, IAV inactivation was calculated in each shell and at each time point, and the residual virus concentration was integrated over the entire droplet. The resulting inactivation curves correspond well to the measured data in all droplets investigated (**Figure 3G-J**). The model was able to capture the inverted sigmoidal curve of the inactivation in effloresced droplets, the first-order inactivation in deliquesced droplets, and was able to reproduce the protective effect of sucrose.

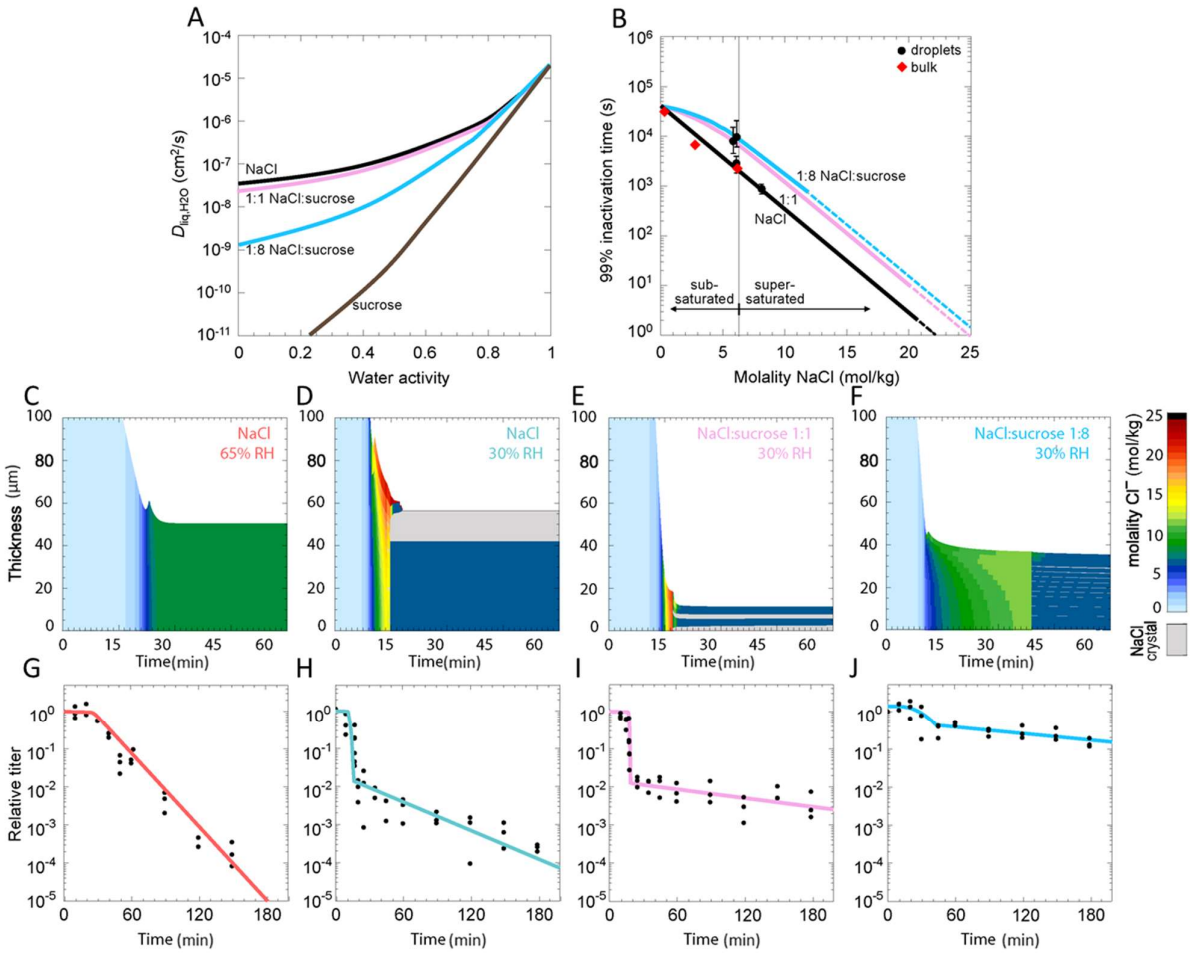

Figure 3: IAV inactivation in deposited droplets modeled with ResAM. (A) Liquid phase diffusion coefficients of H_2O molecules in aqueous NaCl and sucrose solutions and 1:1 and 1:8 dry mass ratio mixtures thereof (see Equations S1 to S3). (B) Time required for 99% titer reduction of IAV versus NaCl molality in aqueous NaCl/sucrose droplets derived by fitting ResAM to the experimental data in panels (G)-(J) and in bulk NaCl solutions. The inactivation times in droplets are based on the first order inactivation rates after droplet compositions stopped changing by equilibration with air, that is ≥ 40 min after deposition. The black line represents the model prediction of 99%-inactivation time according to **Equation 3** for NaCl only. The blue and green lines are for aqueous NaCl:sucrose mixtures with a dry mass ratio of 1:1 and 1:8, respectively, according to **Equation 4**. (C)-(F) Evolution of NaCl molality in 1-µl drying droplets with different compositions, modeled with ResAM. At 30% RH, all the droplets reach a final molality of 6.1 *m*, corresponding to saturation conditions after efflorescence independent on sucrose content. Light gray regions show the effloresced NaCl crystals, which are modeled as dendrites with average distances of 5 um, as observed by Luo et al.[27] in synthetic lung fluid. In (D) a crust of pure salt hinders the further diffusion of H_2O, whereas in (E)-(F) the (assumed) salt layers interspersed with sucrose reduce the aqueous NaCl concentration but remain penetrable for H_2O molecules. (G)-(J) Measured IAV inactivation in 1-µl droplets (black dots) in NaCl at 65% RH (G), NaCl at 30% RH (H), NaCl:sucrose 1:1 at 30% RH (I) and NaCl:sucrose 1:8 at 30% RH (J) and simulated inactivation curve (solid lines) determined using ResAM.

Effect of NaCl on infection cycle and virion integrity

To gain insight into the mechanism of NaCl-induced inactivation, we first conducted fluorescence imaging of viral replication within cells (see Supporting Methods). For this purpose, we used sample aliquots from the inactivation experiment in 1-µl NaCl droplets exposed to 30% or 65% RH (**Figure 2A**). At both RH levels, the IAV titer was reduced by ~3-$\log_{10}$ after 120 min. Samples taken at times 0 and 120 min ("t0" and "t120", respectively) were used to infect A549 cells for 6 h, prior to fluorescent staining of the IAV nucleoprotein (NP). A549 cell nuclei were stained with DAPI. Fluorescence microscopy showed that in cells infected with viruses in freshly deposited droplets (exposure time 0 min), NP production was present in approximately half of the cells (**Figure 4A**), indicating that viral replication occurred. However, viruses exposed to 30% or 65% RH for 120 min did not show any NP signal 6 h post infection, indicating that the infection cycle was interrupted at an early stage (that is, before the onset of NP protein synthesis).

Next, we investigated the integrity of the virions after droplet drying (see Supporting Methods). To this end, 1-µl NaCl droplets were again exposed to 30 and 65% RH, resulting in 1.5-2.5 $\log_{10}$ inactivation after 120 min (**Figure 4B-C**). The t0 and t120 samples were then incubated for 30 min at 37°C in a digestion mixture (see composition in *Methods*) containing RNase, and the residual RNA copy number was subsequently quantified by RT-qPCR. Hereby the assumption is that if the virion integrity is compromised by exposure to NaCl, the RNase can access and degrade the viral RNA, whereas in intact virions, the RNA is protected.[46] As a control, half the volume of each sample was exposed to the digestion mixture without RNase. In the absence of RNAse, only a minor loss of genome copies was observed between t0 and t120. In contrast, in the presence of RNAse, the t120 sample exhibited approximately a 2-$\log_{10}$ decrease in genomic copies compared to the t0 sample at both humidities (**Figure 4B-C**). This decay corresponds well to the observed infectivity decay (**Figure 4B-C**), suggesting that the disruption of virion integrity is the main inactivation mechanism at high NaCl concentrations.

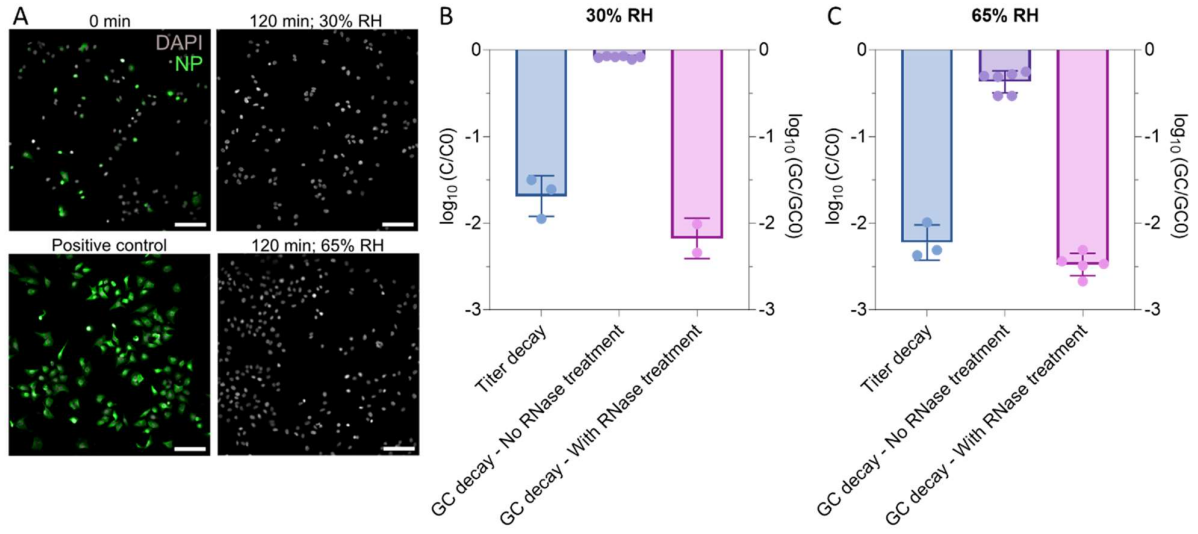

Figure 4: Effect of high salinity on IAV infectivity. (A) Immunofluorescence images of A549 cells infected with IAV samples exposed to 30% or 65% RH in 1-µl NaCl droplets for 120 min. A549 cells were infected at a multiplicity of infection (MOI) of 1, and IAV protein production was visualized by immunofluorescent staining of nucleoprotein at 6 h post-infection. Scale bar corresponds to 100 µm. Images are representative of duplicate experiments. The positive control was infected with a fresh stock of IAV. (B,C) Infectivity decay of IAV samples exposed to 30% (B) or 65% RH (C) in 1-µl NaCl droplets for 120 min, and genome quantification by RT-qPCR of these samples incubated with and without RNase for 30 min prior to RNA extraction. Data are presented as the $\log_{10}$ of the ratio between viral concentration after 120-min exposure in droplet and the initial concentration. In case of infectivity measurements, the virus concentration is represented by the titer (in PFU/ml), and in case of RT-qPCR quantification, the virus concentration is represented by the genomic copies (in GC/ml).

Discussion

Salinity has been proposed as a promoter for the inactivation of viruses,[47–49] yet a comprehensive understanding of the underlying mechanisms and kinetics has remained elusive. In this study, we combined experimental data on IAV inactivation at different salinities with a biophysical model to parameterize the effect of NaCl on virus stability. Our data suggest that the main inactivation driver of IAV in saline droplets is exposure to high NaCl molality rather than the formation of salt crystals during efflorescence. This suggestion was confirmed by model simulations showing that the NaCl molality, which changes within the droplet over time, is sufficient to explain the observed inactivation.

The ResAM model was able to capture the entire inactivation curve observed in both effloresced and deliquesced droplets, and in both aqueous NaCl and NaCl/sucrose matrices. A recent study proposed the inactivation of bacteriophage MS2 to be correlated with the cumulative dose, defined as the solute concentration multiplied by the exposure time.[19] A dose-dependent inactivation could not be confirmed by ResAM for IAV. Instead, we here demonstrate an exponential dependence of IAV inactivation on salt molality, suggesting that an increase in molality leads to a disproportionate increase in inactivation. In particular at salt molalities > 20 *m*, inactivation times become very fast, with 99% inactivation achieved within seconds. However, even at a RH as low as 30%, it takes several minutes to reach such molalities in 1-µl NaCl droplets, and in droplets containing large amounts of organics, such molalities may not be reached at all.

While we found that salinity promotes IAV inactivation in millimeter-sized droplets, virus inactivation was suggested to be driven by acidic[27] or basic[50] pH in aerosol particles with diameters up to few micrometers. Acidification in millimeter-sized droplets is, however, too slow to compete with salt-mediated inactivation, [27] and we found IAV to be stable over the course of 1 h at an alkaline pH of 11 (**Figure S7**). Here we can thus exclude pH as a determinant of virus inactivation, highlighting the importance of salinity in modulating virus stability in millimeter-sized droplets. Depending on the organic content, the salinity increase in the droplets may be limited and the virus may remain stable for hours. Therefore, droplet transmission may play an important role in the spread of IAV, and a combination of prevention strategies addressing both aerosol (e.g. ventilation) and droplet transmission (e.g. surface disinfection), may be needed to prevent the spread of influenza.

The inactivation of IAV in drying droplets may be explained by a combined effect of two processes: the removal of water molecules due to evaporation, and the subsequent increase of salt molality. Our data suggest that the virion integrity is damaged in drying NaCl droplets (**Figure 4**). Virion integrity loss was also observed to be a minor mechanism in the inactivation of IAV by acidic pH, as encountered in small aerosol particles.[46] For salinity-mediated inactivation in drying droplets, however, damage to the virus structure seems to be the main inactivation mechanism. Therefore, we here summarize how these two processes may affect the lipid envelope and the viral proteins.

Upon drying, the osmotic pressure induced by the solutes increases and causes shrinkage of IAV by forcing water molecules to exit the virus.[51] The shrinkage rate constant of influenza virus was previously observed to increase with ionic strength, until reaching a threshold where the lipids and the matrix proteins (M1) are no longer able to adapt to the compressive stress, resulting in morphological change and loss of membrane integrity.[51] This concurs with our finding that damage to the viral integrity is the main inactivation mechanism. The authors furthermore hypothesize that the morphological change in the membrane leads to irreversible conformational changes, resulting in the loss of hemagglutinin (HA) activity. We did not investigate the structural integrity and functionality of HA in this work, though it is possible that this mechanism occurs concomitantly to the loss of virion integrity in drying saline droplets.

In addition to osmotic stress, water evaporation may induce leakage of the viral lipid envelope. It was shown that when the water molecules surrounding the phosphate heads of membrane phospholipids are removed, the packing of the head groups densifies. The subsequent increase of Van der Waals' interactions among hydrocarbon chains trigger a phase transition in the lipid bilayer.[52,53] Specifically, under physiological conditions, the phase transition temperature, (T_m) is usually below room temperature, and the hydrated lipids are in a disordered, flexible liquid crystalline phase. However, the increase of Van der Waals' interactions due to water removal increases T_m to values above room temperature and forces the dried lipids to transition into an ordered, solid-like gel phase. Upon rehydration, the lipids then undergo a reverse phase transition when the head group packing decreases due to the formation of H-bonds with water. These phase transitions induce leakage of the lipid bilayer, damaging the membrane. We hypothesize that a similar mechanism occurs in the viral envelope of influenza virus in a drying droplet or aerosol particle, with rehydration occurring when the particle is inhaled by a host. Moreover, both Na^+ and Cl^- ions were found to bind with the lipid head groups, increasing the ordering of the lipids and subsequently increasing T_m.[54–57] We propose that the combination of water removal and NaCl attachment to the lipid bilayer promote phase transition and cause damage to the viral envelope, which may interfere with fusion during viral infection. Such a mechanism agrees with our data that demonstrate that in drying droplets, IAV inactivation is driven by high NaCl molality and is caused by damaging the virion integrity. It is also consistent with findings by Lin et al.,[58] who observed a higher salt susceptibility of the enveloped bacteriophage Φ6 than the non-enveloped bacteriophage MS2, supporting the hypothesis of viral envelope disruption by high salinity. Similarly, Kukkaro and Bamford[59] saw a larger sensitivity to NaCl concentration changes of enveloped viruses compared to non-enveloped ones. Nevertheless, to conclusively confirm this mechanism, future work should study phase transition mechanism in the lipid bilayers of enveloped viruses in drying droplets.

We observed that the addition of sucrose is protective for IAV in drying droplets (**Figure 2C**). The protective mechanism by sucrose is two-fold. First, as shown in **Figure 3**, the presence of sucrose in the matrix decreases the molality of NaCl during the drying phase, thereby lowering viral inactivation. This effect is particularly evident at an NaCl:sucrose ratio of 1:8, and constitutes an indirect protective effect from sucrose. Second,

our results show thatsucrose also has a direct protective mechanism: in droplets at equilibrium, the NaCl molality is independent of the sucrose concentration (**Figure 3B**), and yet lower inactivation rate constants are observed when sucrose is present (**Table S2**). The inactivation rate constants follow the trend 1:0 > 1:1 > 1:8 (**Figure 3H-J**), showing that an increasing sucrose concentration increases the protection. Here, the protection cannot be attributed to a change in NaCl molality, as the latter is at saturation in all conditions. Therefore, a different, direct mechanism must protect the virus.

Potential direct protection mechanisms by sucrose acting on both lipids and proteins are described in the literature. The addition of disaccharides, such as sucrose and trehalose, was previously shown to help stabilize the membrane phospholipids during lyophilization.[52,53,60] The sugar molecules interact with the phosphates, inserting in between the head groups and replacing water. The packing density needs to decrease to give room to the sugars, and the Van der Waals' interactions are reduced. Consequently, T_m is decreased, and remains below room temperature. Therefore, despite water removal, the lipids do not undergo phase transition, and no membrane leakage occurs. The direct protection of IAV exerted by sucrose in the droplet may thus be partly due to the protection of the lipid bilayer from water loss, preventing the damage to the lipid envelope during drying. In addition, the sucrose may also protect the lipid bilayer from the effects of salt, if sucrose replaces the Na^+ and Cl^- ions between the lipid head groups and thereby counteracts the increase in T_m caused by the salt. This mechanism remains to be assessed, but it correlates with the decrease in inactivation rate as a function of sucrose content in matrices with similar NaCl molalities (**Figure 3H-J**).

Additionally, protection may arise from the stabilization of surface proteins by sucrose.[61–64] Upon drying, the water molecules stabilizing the structure of proteins are removed, unfolding the proteins and inducing potentially irreversible conformational changes.[62,65] However, when osmolytes (here, sucrose) are present, they are sterically excluded from the first hydration shell of the proteins. This preferential exclusion of the sucrose leads to a preferential hydration of the proteins, increasing the free energy of the system. The unfolded state of the proteins becomes thermodynamically unfavorable, forcing the proteins to remain in their native state. Our data do not indicate whether protein unfolding occurred in drying droplets, and therefore we cannot assess whether the sucrose protection is in fact caused by protein stabilization. Indeed, the surface proteins of a virus have lower mobility than proteins in solution, and it is possible that this stabilization mechanism is less pronounced in viruses. Further studies on IAV are required to confirm this protection mechanism by sucrose and other organics present in respiratory fluids.

This study has some important limitations. First, the ResAM model used herein relies on some assumptions that remain to be validated. Specifically, the encapsulation of residual water and viruses by NaCl crystals in efflorescing droplets, as well as the formation of micro-crystals in the 1:8 NaCl:sucrose solution, are hypothetical physical processes that need to be assessed. However, previous studies have shown that the viscosity of an organic phase can kinetically limit the coalescence of the inorganic salt crystal,[66] and non-

coalesced salt crystals were observed in porcine respiratory fluid,[67] which supports the hypothesis of micro-crystal formation when the sucrose content is large. We accounted for the flattened shape of the droplet despite using a spherical model by limiting the diffusion depth to the thickness of the spread droplet. This represents also an uncertainty of ResAM. Finally, the simple NaCl/sucrose/water matrices that were used in this study are useful to parameterize ResAM, but are far less complex than real respiratory fluids and saliva. In real matrices, other processes may occur during droplet drying, such as the formation of a glassy shell by proteins, limiting evaporation.[31] In addition, the morphology of the dried droplet, the importance of which has been recently presented by Rockey et al.,[38] is dependent on the matrix composition, such as the Na:K mass ratio[67] and the initial NaCl content[33,34] that can affect crystal formation. It is therefore essential to combine the study of both simple and more complex matrices, to entangle the effect of all parameters and assess their importance for IAV transmission.

In summary, we demonstrate that IAV inactivation in deposited droplets is driven by the high NaCl molality due to water evaporation, rather than the physical formation of the crystal. We furthermore propose a model to simulate IAV inactivation in droplets as a function of RH, NaCl and organic concentration. Finally, we determined that organics (sucrose) protect IAV by two mechanisms: first by decreasing the salt molality in the drying droplet, and second by a direct mechanism that may prevent the leakage of the lipid bilayer and the unfolding of surface proteins. This work helps to understand and quantify virus inactivation in drying droplets, thereby increasing the fundamental knowledge of airborne virus transmission that is essential to design relevant mitigation strategies.

References

1. Tellier, R. Aerosol transmission of influenza A virus: a review of new studies. *J. R. Soc. Interface* **6**, S783–S790 (2009).

2. Cowling, B. J. *et al.* Aerosol transmission is an important mode of influenza A virus spread. *Nat. Commun.* **4**, 1935 (2013).

3. Koster, F. *et al.* Exhaled aerosol transmission of pandemic and seasonal H1N1 influenza viruses in the ferret. *PLoS One* **7**, e33118 (2012).

4. Yan, J. *et al.* Infectious virus in exhaled breath of symptomatic seasonal influenza cases from a college community. *PNAS* **115**, 1081–1086 (2018).

5. Bischoff, W. E., Swett, K., Leng, I. & Peters, T. R. Exposure to influenza virus aerosols during routine patient care. *J. Infect. Dis.* **207**, 1037–1046 (2013).

6. Tellier, R. Review of aerosol transmission of influenza A virus. *Emerg. Infect. Dis.* **12**, 1657–1662 (2006).

7. Dhawan, S. & Biswas, P. Aerosol dynamics model for estimating the risk from short-range airborne transmission and inhalation of expiratory droplets of SARS-CoV-2. *Environ. Sci. Technol.* **55**, 8987–8999 (2021).

8. Verheyen, C. A. & Bourouiba, L. Associations between indoor relative humidity and global COVID-19 outcomes. *J. R. Soc. Interface* **19**, 20210865 (2022).

9. Shechmeister, I. L. Studies on the experimental epidemiology of respiratory infections. III. Certain aspects of the behavior of type A influenza virus as an air-borne cloud. *J. Infect. Dis.* **87**, 128–132 (1950).

10. Hemmes, J. H., Winkler, K. C. & Kool, S. M. Virus survival as a seasonal factor in influenza and poliomyelitis. *Nature* **28**, 221–233 (1962).

11. Yang, W. & Marr, L. C. Dynamics of Airborne influenza A viruses indoors and dependence on humidity. *PLoS One* **6**, e21481 (2011).

12. Marr, L. C., Tang, J. W., Van Mullekom, J. & Lakdawala, S. S. Mechanistic insights into the effect of humidity on airborne influenza virus survival, transmission and incidence. *J. R. Soc. Interface* **16**, 20180298 (2019).

13. Harper, G. J. Airborne micro-organisms: survival tests with four viruses. *J. Hyg. (Lond).* **59**, 479–486 (1961).

14. Schaffer, F. L., Soergel, M. E. & Straube, D. C. Survival of airborne influenza virus: effects of propagating host, relative humidity, and composition of spray fluids. *Arch. Virol.* **51**, 263–273 (1976).

15. Schuit, M. *et al.* The influence of simulated sunlight on the inactivation of influenza virus in aerosols. *J. Infect. Dis.* **221**, 372–378 (2020).

16. Schuit, M. *et al.* Airborne SARS-CoV-2 is rapidly inactivated by simulated sunlight. *J. Infect. Dis.* **222**, 564–571 (2020).

17. Ijaz, M. K., Brunner, A. H., Sattar, S. A., Nair, R. C. & Johnson-Lussenburg, C. M. Survival characteristics of airborne human coronavirus 229E. *J. Gen. Virol.* **66**, 2743–2748 (1985).

18. Dabisch, P. *et al.* The influence of temperature, humidity, and simulated sunlight on the infectivity of SARS-CoV-2 in aerosols. *Aerosol Sci. Technol.* **55**, 142–153 (2021).

19. Lin, K. & Marr, L. C. Humidity-dependent decay of viruses, but not bacteria, in aerosols and droplets follows disinfection kinetics. *Environ. Sci. Technol.* **54**, 1024–1032 (2020).

20. Morris, D. H. *et al.* Mechanistic theory predicts the effects of temperature and humidity on inactivation of SARS-CoV-2 and other enveloped viruses. *eLife* **10**, e65902 (2021).

21. Ahlawat, A. *et al.* Impact of chemical properties of human respiratory droplets and aerosol particles on airborne viruses' viability and indoor transmission. *Viruses* **14**, 1497 (2022).

22. Oswin, H. *et al.* Measuring stability of virus in aerosols under varying environmental conditions. *Aerosol Sci. Technol.* **5**, 1315–1320 (2021).

23. French, A. J. *et al.* Environmental stability of enveloped viruses is impacted by the initial volume and evaporation kinetics of droplets. *mBio* **14**, e03452-22 (2023).

24. Huang, Q., Wang, W. & Vikesland, P. J. Implications of the coffee-ring effect on virus infectivity. *Langmuir* **37**, 11260–11268 (2021).

25. Klein, L. K. *et al.* Expiratory aerosol pH is determined by indoor room trace gases and particle size. *PNAS* **119**, e2212140119 (2022).

26. Ciobanu, V. G., Marcolli, C., Krieger, U. K., Weers, U. & Peter, T. Liquid-liquid phase separation in mixed organic/inorganic aerosol particles. *J. Phys. Chem. A* **113**, 10966–10978 (2009).

27. Luo, B. *et al.* Expiratory aerosol pH: the overlooked driver of airborne virus inactivation. *Environ. Sci. Technol.* **57**, 486–497 (2023).

28. Schaub, A. Expiratory aerosol pH is a driver of the persistence of airborne influenza A virus. *Chimia* **77**, 196–200 (2023).

29. Yang, W., Elankumaran, S. & Marr, L. C. Relationship between humidity and influenza A viability in droplets and implications for influenza's seasonality. *PLoS One* **7**, e46789 (2012).

30. Peng, C., Chen, L. & Tang, M. A database for deliquescence and efflorescence relative humidities of compounds with atmospheric relevance. *Fundam. Res.* **2**, 578–587 (2022).

31. Niazi, S. *et al.* Humidity-dependent survival of an airborne influenza A virus: Practical implications for controlling airborne viruses. *Environ. Sci. Technol. Lett.* **8**, 412–418 (2021).

32. Niazi, S. *et al.* Susceptibility of an airborne common cold virus to relative humidity. *Environ. Sci. Technol.* **55**, 499–508 (2021).

33. Haddrell, A. *et al.* Ambient carbon dioxide concentration correlates with SARS-CoV-2 aerostability and infection risk. *Res. Sq.* **preprint**, (2023).

34. Haddrell, A. *et al.* Differences in airborne stability of SARS-CoV-2 variants of concern is impacted by alkalinity of surrogates of respiratory aerosol. *Interface* **20**, 20230062 (2023).

35. Kormuth, K. A. *et al.* Influenza virus infectivity is retained in aerosols and droplets independent of relative humidity. *J. Infect. Dis.* **218**, 739–747 (2018).

36. Kong, Z. *et al.* Virus dynamics and decay in evaporating human saliva droplets on fomites. *Environ. Sci. Technol.* 2c02311 (2022).

37. Malamud, D. *et al.* Antiviral activities in human saliva. *Adv. Dent. Res.* **23**, 34–37 (2011).

38. Rockey, N. C., Le Sage, V., Marr, L. C. & Lakdawala, S. S. Seasonal influenza viruses decay more rapidly at intermediate humidity in droplets containing saliva compared to respiratory mucus. *bioRxiv* **preprint**, 2023–07 (2023).

39. Pöhlker, M. L. *et al.* Respiratory aerosols and droplets in the transmission of infectious diseases. *Rev. Mod. Phys.* **95**, 045001 (2023).

40. Bustin, S. A. *et al.* The MIQE guidelines: minimum information for publication of quantitative real-time PCR experiments. *Clin. Chem.* **55**, 611–622 (2009).

41. Choi, H. J. *et al.* Stability of influenza vaccine coated onto microneedles. *Biomaterials* **33**, 3756–3769 (2012).

42. Quan, F., Rubino, I., Lee, S., Koch, B. & Choi, H.-J. Universal and reusable virus deactivation system for respiratory protection. *Sci. Rep.* **7**, 39956 (2017).

43. Mattle, M. J. *et al.* Impact of virus aggregation on inactivation by peracetic acid and implications for other disinfectants. *Environ. Sci. Technol.* **45**, 7710–7717 (2011).

44. Sharp, D. G., Floyd, R. & Johnson, J. D. Nature of the surviving plaque-forming unit of reovirus in water containing bromine. *Appl. Microbiol.* **29**, 94–101 (1975).

45. Lenzi, F., Tran, T.-T. & Teng, T.-T. The water-activity of supersaturated aqueous solutions of NaCl, KCl, and K_2SO_4 at 25° C. *Can. J. Chem.* **53**, 3133–3140 (1975).

46. David, S. C. *et al.* Inactivation mechanisms of influenza A virus under pH conditions encountered in aerosol particles as revealed by whole-virus HDX-MS. *mSphere* **8**, e00226-23 (2023).

47. Brown, J. D., Goekjian, G., Poulson, R., Valeika, S. & Stallknecht, D. E. Avian influenza virus in water: infectivity is dependent on pH, salinity and temperature. *Vet. Microbiol.* **136**, 20–26 (2009).

48. Benbough, J. E. Some factors affecting the survival of airborne viruses. *J. Gen. Virol.* **10**, 209–220 (1971).

49. Salo, R. J. & Cliver, D. O. Effect of acid pH, salts, and temperature on the infectivity and physical integrity of enteroviruses. *Arch. Virol.* **52**, 269–282 (1976).

50. Oswin, H. P. *et al.* The dynamics of SARS-CoV-2 infectivity with changes in aerosol microenvironment. *PNAS* **119**, e2200109119 (2022).

51. Choi, H. J. *et al.* Effect of osmotic pressure on the stability of whole inactivated influenza vaccine for coating on microneedles. *PLoS One* **10**, e0134431 (2015).

52. Crowe, J. H., Hoekstra, F. A. & Crowe, L. M. Anhydrobiosis. *Annu. Rev. Physiol.* **54**, 579–599 (1992).

53. Rockinger, U., Funk, M. & Winter, G. Current approaches of preservation of cells during (freeze-) drying. *J. Pharm. Sci.* **110**, 2873–2893 (2021).

54. Lee, S. J., Song, Y. & Baker, N. A. Molecular dynamics simulations of asymmetric NaCl and KCl solutions separated by phosphatidylcholine bilayers: Potential drops and structural changes induced by strong Na^+-lipid interactions and finite size effects. *Biophys. J.* **94**, 3565–3576 (2008).

55. Pabst, G. *et al.* Rigidification of neutral lipid bilayers in the presence of salts. *Biophys. J.* **93**, 2688–2696 (2007).

56. Pandit, S. A., Bostick, D. & Berkowitz, M. L. Molecular dynamics simulation of a dipalmitoylphosphatidylcholine bilayer with NaCl. *Biophys. J.* **84**, 3743–3750 (2003).

57. Valley, C. C., Perlmutter, J. D., Braun, A. R. & Sachs, J. N. NaCl interactions with phosphatidylcholine bilayers do not alter membrane structure but induce long-range ordering of ions and water. *J. Membr. Biol.* **244**, 35–42 (2011).

58. Lin, K., Schulte, C. R. & Marr, L. C. Survival of MS2 and Φ6 viruses in droplets as a function of relative

humidity, pH, and salt, protein, and surfactant concentrations. *PLoS ONE* **15**, (2020).

59. Kukkaro, P. & Bamford, D. H. Virus-host interactions in environments with a wide range of ionic strengths. *Environ. Microbiol. Rep.* **1**, 71–77 (2009).

60. Chen, C., Han, D., Cai, C. & Tang, X. An overview of liposome lyophilization and its future potential. *J. Control. Release* **142**, 299–311 (2010).

61. Liu, F. F., Ji, L., Zhang, L., Dong, X. Y. & Sun, Y. Molecular basis for polyol-induced protein stability revealed by molecular dynamics simulations. *J. Chem. Phys.* **132**, 225103 (2010).

62. Singh, S. K. Sucrose and trehalose in therapeutic protein formulations. in *Challenges in Protein Product Development* 63–95 (2018).

63. Timasheff, S. N. The control of protein stability and association by weak interactions with water: how do solvents affect these processes. *Annu. Rev. Biophys. Biomol. Struct.* **22**, 67–97 (1993).

64. Lee, J. C. & Timasheff, S. N. The stabilization of proteins by sucrose. *J. Biol. Chem.* **256**, 7193–7201 (1981).

65. Minhaz Ud-Dean, S. M. Structural explanation for the effect of humidity on persistence of airborne virus: Seasonality of influenza. *J. Theor. Biol.* **264**, 822–829 (2010).

66. Fard, M. M., Krieger, U. K. & Peter, T. Kinetic limitation to inorganic ion diffusivity and to coalescence of inorganic inclusions in viscous liquid-liquid phase-separated particles. *J. Phys. Chem. A* **121**, 9284–9296 (2017).

67. Groth, R., Niazi, S., Spann, K., Johnson, G. R. & Ristovski, Z. Physicochemical characterization of porcine respiratory aerosol and considerations for future aerovirology. *PNAS Nexus* **2**, 1–10 (2023).

Funding

Swiss National Science Foundation grant 189939 (TK, AN, SSt, UKK)

Author contributions statement

Conceptualization: AS, TK, TP, UKK

Methodology: AS, BL, IG, LKK, SCD, TK, TP, UKK

Software: BL

Formal analysis: AS, BL, TP

Investigation: AS, BL, IG, LC, SCD

Resources: UKK, SSt, TK

Writing–original draft: AS, BL, TK, TP

Writing–review & editing: AS, BL, CT, GM, IG, KV, LKK, MP, NB, SCD, SSt, TP, TK, UKK

Visualization: AS, BL, IG, LKK, TK, TP

Supervision: SSt, TK, TP, UKK

Project administration: TK

Funding acquisition: AN, SSt, TK, TP, UKK, WH

Competing interests

Authors declare that they have no competing interests.

Data and material availability

Experimental data are available in the public repository Zenodo under the following link: https://zenodo.org/records/10418730. ResAM code will be made available upon manuscript acceptance.